Appl. Math. Mech. -Engl. Ed., **44**(3), 411–430 (2023)

APPLIED MATHEMATICS AND MECHANICS (ENGLISH EDITION)

https://doi.org/10.1007/s10483-023-2958-8

Complete solutions for elastic fields induced by point load vector in functionally graded material model with transverse isotropy*

Sha XIAO[1], Zhongqi YUE[2,†]

1. Key Laboratory of Urban Security and Disaster Engineering of China Ministry of Education, Beijing University of Technology, Beijing 100124, China;
2. Department of Civil Engineering, The University of Hong Kong, Hong Kong, China

(Received Aug. 29, 2022 / Revised Nov. 9, 2022)

Abstract The paper develops and examines the complete solutions for the elastic field induced by the point load vector in a general functionally graded material (FGM) model with transverse isotropy. The FGMs are approximated with n-layered materials. Each of the n-layered materials is homogeneous and transversely isotropic. The complete solutions of the displacement and stress fields are explicitly expressed in the forms of fifteen classical Hankel transform integrals with ten kernel functions. The ten kernel functions are explicitly expressed in the forms of backward transfer matrices and have clear mathematical properties. The singular terms of the complete solutions are analytically isolated and expressed in exact closed forms in terms of elementary harmonic functions. Numerical results show that the computation of the complete solutions can be achieved with high accuracy and efficiency.

Key words functionally graded material (FGM), transverse isotropy, elasticity, closed-form singular solution, Green's function, point load vector

Chinese Library Classification O175.8, O343.7
2010 Mathematics Subject Classification 35A08, 35G60

1 Introduction

Functionally graded materials (FGMs) have the elastic properties varying with the depth and can keep the properties constant along the horizontal direction. They can be approximated and represented by the n-layered FGM model shown in Fig. 1, where n is an arbitrary positive integer and stands for the total number of the material layers. The n-layered FGM model can occupy the full three-dimensional (3D) space by further adhering two materials of either upper or lower semi-infinite extent. Each individual layer is homogeneous and has five elastic

* Citation: XIAO, S. and YUE, Z. Q. Complete solutions for elastic fields induced by point load vector in functionally graded material model with transverse isotropy. *Applied Mathematics and Mechanics* (*English Edition*), **44**(3), 411–430 (2023) https://doi.org/10.1007/s10483-023-2958-8

† Corresponding author, E-mail: yueqzq@hku.hk

Project supported by the National Natural Science Foundation of China (No. 42207182) and the Research Grants Council of the Hong Kong Special Administrative Region Government of China (Nos. HKU 17207518 and R5037-18)

parameters of transverse isotropy. The five elastic parameters can be noted as $c_{1j}, c_{2j}, c_{3j}, c_{4j}$, and c_{5j}, where $j = 0, 1, 2, \cdots, n, n+1$. The interfacial conditions between any two connected dissimilar layers are fully bonded, where the three displacements and the three vertical stresses acting on any interface plane are continuous.

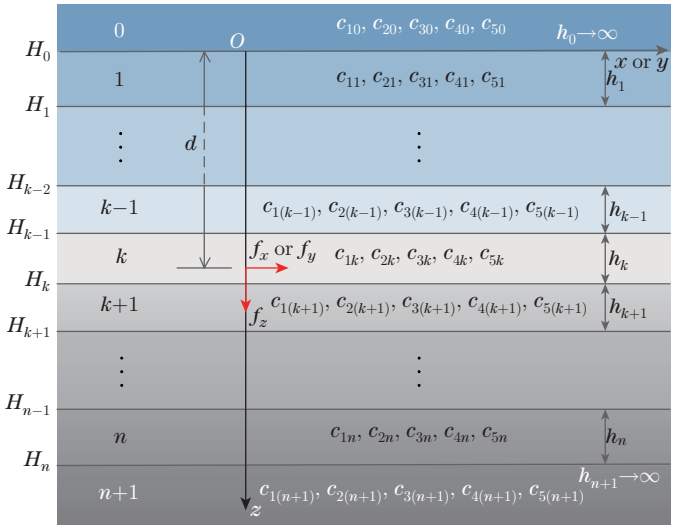

Fig. 1 Schematics of n-layered FGM model with isotropy or transverse isotropy of full-space subject to point load vector (f_x, f_y, f_z) (color online)

There are the following characteristics: (i) The upper material of $-\infty < z \leqslant H_0^-$ is the 0th homogeneous elastic half-space; (ii) The layer material of $H_{j-1}^+ < z \leqslant H_j^-$ $(j = 1, 2, \cdots, n)$ is the jth homogeneous elastic layer with the layer thickness $h_j = H_j - H_{j-1}$; (iii) The lower material of $H_n^+ \leqslant z < +\infty$ is the $(n+1)$th homogeneous elastic half-space. As n can be large, the above n-layered FGM model has its five elastic parameters varying with the depth as a stepped function, and can well represent the arbitrary variations of any general FGM elastic parameters with the depth.

Without loss of generality, the point load vector is concentrated at an arbitrary horizontal plane $z = d$ in the n-layered FGM model,

$$\boldsymbol{f}(x, y, z) = \boldsymbol{f}_{\mathrm{c}} \delta(x)\delta(y)\delta(z - d), \tag{1}$$

where $H_{k-1}^+ \leqslant d \leqslant H_k^-$ $(1 \leqslant k \leqslant n)$, δ is a Dirac delta function, and $\boldsymbol{f}_{\mathrm{c}} = (f_x, f_y, f_z)^{\mathrm{T}}$. In particular, the loading situation for $-\infty < d \leqslant H_0$ or $H_n^+ < d < +\infty$ can be included by dividing a single layer of finite thickness $h > H_0 - d$ or $h > d - H_n$ in the 0th or $(n+1)$th layer, respectively.

The above boundary value problem is an extension of the classical problems related to the fundamental singularity or Green's function or point load solutions in elasticity[1–16]. Pan[14] documented the relevant publications in general Green's functions. Yue[17] derived the fundamental singular solutions of elastic fields in the n-layered isotropic elastic material subject to two body force vectors. The past papers[12,17–21] examined the mathematical methods for the solutions of elastostatics in n-layered dissimilar elastic materials, and the methods were used by other researchers including Merkel et al.[22] and Maloney et al.[23]. Xiao and Yue[24] used the point load solutions of the n-layered FGM model with isotropy[17], and developed the boundary element methods for analyzing the fracture mechanics and contact mechanics in

layered and graded materials. This paper aims to concisely and explicitly derive and present the complete solutions with closed-form singularity and to further present its accurate computational method for the elastic field induced by a point load vector in the n-layered FGM model with either isotropy or transverse isotropy. The numerical results with pre-given accuracy of convergence are obtained for the elastic field at any point in the FGM model, and the influence of heterogeneity and anisotropy on the elastic fields is illustrated.

2 General solutions in FGM model with transverse isotropy

2.1 Governing equations

In the jth layer of the n-layered FGM model (see Fig. 1), the linear constitutive equations governing the stresses (σ_{ij}) and the strains (ε_{ij}) take the forms of

$$\begin{cases} \sigma_{xx} = c_{1j}\varepsilon_{xx} + (c_{1j} - 2c_{5j})\varepsilon_{yy} + c_{2j}\varepsilon_{zz}, \quad \sigma_{yy} = (c_{1j} - 2c_{5j})\varepsilon_{xx} + c_{1j}\varepsilon_{yy} + c_{2j}\varepsilon_{zz}, \\ \sigma_{zz} = c_{2j}\varepsilon_{xx} + c_{2j}\varepsilon_{yy} + c_{3j}\varepsilon_{zz}, \quad \sigma_{xz} = 2c_{4j}\varepsilon_{xz}, \quad \sigma_{yz} = 2c_{4j}\varepsilon_{yz}, \quad \sigma_{xy} = 2c_{5j}\varepsilon_{xy}. \end{cases} \tag{2}$$

For the special case of an isotropic elastic material, where

$$\Delta_j = \sqrt{c_{1j}c_{3j}} - c_{2j} - 2c_{4j} = 0,$$

the five parameters can be reduced to the Lamé constants λ_j and μ_j, i.e.,

$$c_{2j} = \lambda_j, \quad c_{4j} = c_{5j} = \mu_j, \quad c_{1j} = c_{3j} = \lambda_j + 2\mu_j.$$

By the definition of positive strain energy in elastic materials, we have the constraints on the five elastic parameters as follows:

$$c_{1j} > c_{5j} > 0, \quad c_{3j} > 0, \quad c_{4j} > 0, \quad \sqrt{c_{1j}c_{3j}} > c_{2j}. \tag{3}$$

The strains are related to the displacements, which can be expressed as

$$\varepsilon_{lm} = \frac{1}{2}(u_{l,m} + u_{m,l}), \quad l, m = x, y, z. \tag{4}$$

The governing equations are complete with the specification of equations of static equilibrium in the open regions of vertically inhomogeneous materials,

$$\sigma_{lm,m} + f_l = 0, \tag{5}$$

where the body force vector f_l is given in Eq. (1).

2.2 Solution representation in matrix Fourier integral transforms

The solutions of the displacement, the vertical stress, and the plane strains can be expressed by

$$\boldsymbol{u} = \begin{pmatrix} u_x \\ u_y \\ u_z \end{pmatrix}, \quad \boldsymbol{T}_z = \begin{pmatrix} \sigma_{xz} \\ \sigma_{yz} \\ \sigma_{zz} \end{pmatrix}, \quad \boldsymbol{\Gamma}_{\mathrm{p}} = \begin{pmatrix} \varepsilon_{xx} \\ \varepsilon_{xy} \\ \varepsilon_{yy} \end{pmatrix}. \tag{6}$$

In the ensuing, the set of solution representations is presented for the field variables in the jth elastic layer ($-\infty < x < +\infty, -\infty < y < +\infty$, and $H_{j-1} \leqslant z \leqslant H_j$) in the Cartesian coordinate systems. Based on the classical theory of Fourier integral transforms, it can be

found that the following set of solution representations exists in Cartesian coordinate systems ($Oxyz$ and $O\xi\eta z$):

$$\begin{cases} \boldsymbol{u}(x,y,z) = \dfrac{1}{2\pi}\displaystyle\int_{-\infty}^{+\infty}\int_{-\infty}^{+\infty}\frac{1}{\rho}\boldsymbol{\Pi}\boldsymbol{w}(\xi,\eta,z)K\mathrm{d}\xi\mathrm{d}\eta, \\ \boldsymbol{T}_z(x,y,z) = \dfrac{1}{2\pi}\displaystyle\int_{-\infty}^{+\infty}\int_{-\infty}^{+\infty}\boldsymbol{\Pi}\boldsymbol{Y}_z(\xi,\eta,z)K\mathrm{d}\xi\mathrm{d}\eta, \\ \boldsymbol{\Gamma}_{\mathrm{p}}(x,y,z) = \dfrac{1}{2\pi}\displaystyle\int_{-\infty}^{+\infty}\int_{-\infty}^{+\infty}\boldsymbol{\Pi}_{\mathrm{p}}\boldsymbol{w}(\xi,\eta,z)K\mathrm{d}\xi\mathrm{d}\eta, \end{cases} \tag{7}$$

where $\rho = \sqrt{\xi^2+\eta^2}$, $K = \mathrm{e}^{\mathrm{i}(\xi x+\eta y)}$, and $\mathrm{i} = \sqrt{-1}$.

In Eq. (7), the above three sets of vectors for the field variables in the physical domain can be represented by two unknown vectors

$$\boldsymbol{w}(\xi,\eta,z) = (w_1,w_2,w_3)^{\mathrm{T}}, \quad \boldsymbol{Y}_z(\xi,\eta,z) = (\tau_1,\tau_2,\tau_3)^{\mathrm{T}}$$

for all the boundary-value problems of a solid occupying the jth layer region of $-\infty < x < +\infty$, $-\infty < y < +\infty$, and $H_{j-1} \leqslant z \leqslant H_j$. The coordinate coefficient matrices $\boldsymbol{\Pi}$ and $\boldsymbol{\Pi}_{\mathrm{p}}$ are defined by

$$\boldsymbol{\Pi} = \frac{1}{\rho}\begin{pmatrix} \mathrm{i}\xi & \mathrm{i}\eta & 0 \\ \mathrm{i}\eta & -\mathrm{i}\xi & 0 \\ 0 & 0 & \rho \end{pmatrix}, \quad \boldsymbol{\Pi}_{\mathrm{p}} = -\frac{1}{\rho^2}\begin{pmatrix} \xi^2 & \xi\eta & 0 \\ \xi\eta & \dfrac{1}{2}(\eta^2-\xi^2) & 0 \\ \eta^2 & -\xi\eta & 0 \end{pmatrix}. \tag{8}$$

The two field variable vectors $\boldsymbol{w}(\xi,\eta,z)$ and $\boldsymbol{Y}_z(\xi,\eta,z)$ in the transform domain are re-expressed by $\boldsymbol{u}(x,y,z)$ and $\boldsymbol{T}_z(x,y,z)$ as follows:

$$\begin{cases} \boldsymbol{w}(\xi,\eta,z) = \dfrac{\rho}{2\pi}\displaystyle\int_{-\infty}^{+\infty}\int_{-\infty}^{+\infty}\boldsymbol{\Pi}^*\boldsymbol{u}(x,y,z)K^*\mathrm{d}x\mathrm{d}y, \\ \boldsymbol{Y}_z(\xi,\eta,z) = \dfrac{1}{2\pi}\displaystyle\int_{-\infty}^{+\infty}\int_{-\infty}^{+\infty}\boldsymbol{\Pi}^*\boldsymbol{T}_z(x,y,z)K^*\mathrm{d}x\mathrm{d}y, \end{cases} \tag{9}$$

where K^* and $\boldsymbol{\Pi}^*$ are the complex conjugates of K and $\boldsymbol{\Pi}$, respectively. The body force vector $\boldsymbol{f}(x,y,z)(=(f_x,f_y,f_z)^{\mathrm{T}})$ and its counterpart $\boldsymbol{g}(\xi,\eta,z)(=(g_1,g_2,g_3)^{\mathrm{T}})$ in the transform domain have the following relations:

$$\begin{cases} \boldsymbol{f}(x,y,z) = \dfrac{1}{2\pi}\displaystyle\int_{-\infty}^{+\infty}\int_{-\infty}^{+\infty}\boldsymbol{\Pi}\boldsymbol{g}(\xi,\eta,z)K\mathrm{d}\xi\mathrm{d}\eta, \\ \boldsymbol{g}(\xi,\eta,z) = \dfrac{1}{2\pi}\displaystyle\int_{-\infty}^{+\infty}\int_{-\infty}^{+\infty}\boldsymbol{\Pi}^*\boldsymbol{f}(x,y,z)K^*\mathrm{d}x\mathrm{d}y. \end{cases} \tag{10}$$

It is noted that the solutions of the plane stresses $(\sigma_{xx},\sigma_{xy},\sigma_{yy})$ and the vertical strains $(\varepsilon_{xz},\varepsilon_{yz},\varepsilon_{zz})$ can be easily obtained from the solutions of the vertical stresses $(\sigma_{xz},\sigma_{yz},\sigma_{zz})$ and the plane strains $(\varepsilon_{xx},\varepsilon_{xy},\varepsilon_{yy})$ using the constitutive equation (1).

2.3 Two sets of governing equations in transform domain

The system of the fifteen linear partial differential equations (2), (4), and (5) for the jth homogeneous layer can be simplified and decoupled into the two sets of the first-order ordinary differential equations in the transform domain. The first set is due to the anti-symmetry about

the z-axis of the fifteen governing equations, and has two linear first-order ordinary differential equations with two field variables as follows:

$$\frac{\mathrm{d}}{\mathrm{d}z}\boldsymbol{V}(z)=\rho\boldsymbol{C}_{vj}\boldsymbol{V}(z)-\boldsymbol{G}_v(z), \tag{11a}$$

where $H_{j-1}\leqslant z\leqslant H_j$, $0\leqslant\rho<+\infty$, $\boldsymbol{V}(z)=(w_2,\tau_2)^{\mathrm{T}}$, and $\boldsymbol{G}_v=(0,g_2)^{\mathrm{T}}$.

The second set is due to the axial symmetry about the z-axis of the fifteen governing equations and has four linear first-order ordinary differential equations with four field variables. It can be expressed as follows:

$$\frac{\mathrm{d}}{\mathrm{d}z}\boldsymbol{U}(z)=\rho\boldsymbol{C}_{uj}\boldsymbol{U}(z)-\boldsymbol{G}_u(z), \tag{11b}$$

where $H_{j-1}\leqslant z\leqslant H_j$, $0\leqslant\rho<+\infty$, $\boldsymbol{U}(z)=(w_1,w_3,\tau_3,\tau_1)^{\mathrm{T}}$, and $\boldsymbol{G}_u=(0,0,g_3,g_1)^{\mathrm{T}}$.

Note that the two coefficient matrices $\boldsymbol{C}_{vj}$ and $\boldsymbol{C}_{uj}$ are given in Appendix A. They contain the five material parameters only, and do not contain ξ, η, and ρ. ρ is the only factor of $\boldsymbol{C}_{vj}$ and $\boldsymbol{C}_{uj}$ in Eqs. (11a) and (11b).

2.4 General solutions of $\boldsymbol{V}(z)$ and $\boldsymbol{U}(z)$

The general matrix solutions for the first set of two linear ordinary differential equations (11a) for the jth homogeneous layer ($H_{j-1}\leqslant z\leqslant H_j$) can be obtained as follows:

$$\boldsymbol{V}(z)=\boldsymbol{A}(z-z_1)\boldsymbol{V}(z_1)-\int_{z_1}^{z}\boldsymbol{A}(z-\varsigma)\boldsymbol{G}_v(\varsigma)\mathrm{d}\varsigma. \tag{12}$$

The first basic square matrix $\boldsymbol{A}(s)$ is defined as follows:

$$\boldsymbol{A}(s)=\boldsymbol{B}_j(\gamma_{0j})\mathrm{e}^{\gamma_{0j}\rho s}+\boldsymbol{B}_j(-\gamma_{0j})\mathrm{e}^{-\gamma_{0j}\rho s}, \tag{13}$$

where $z_1=H_{j-1}$ or $z_1=H_j$, γ_{0j} is the material characteristic root, and $\boldsymbol{B}_j(\chi)$ is the material constant matrix.

Similarly, the general matrix solutions for the second set of four linear ordinary differential equations (11b) for the jth homogeneous layer ($H_{j-1}\leqslant z\leqslant H_j$) can be obtained as follows:

$$\boldsymbol{U}(z)=\boldsymbol{Q}(z-z_1)\boldsymbol{U}(z_1)-\int_{z_1}^{z}\boldsymbol{Q}(z-\varsigma)\boldsymbol{G}_u(\varsigma)\mathrm{d}\varsigma. \tag{14}$$

The second basic square matrix $\boldsymbol{Q}(s)$ is defined as follows:

$$\boldsymbol{Q}(s)=\begin{cases}\boldsymbol{C}_j(\gamma_{1j})\mathrm{e}^{\gamma_{1j}\rho s}-\boldsymbol{C}_j(\gamma_{2j})\mathrm{e}^{\gamma_{2j}\rho s}+\boldsymbol{C}_j(-\gamma_{1j})\mathrm{e}^{-\gamma_{1j}\rho s}-\boldsymbol{C}_j(-\gamma_{2j})\mathrm{e}^{-\gamma_{2j}\rho s} & \text{for}\quad \Delta_j>0,\\ \boldsymbol{D}_j(\gamma_{3j})\mathrm{e}^{\gamma_{3j}\rho s}+\boldsymbol{D}_j(-\gamma_{3j})\mathrm{e}^{-\gamma_{3j}\rho s} & \\ \quad+\gamma_{3j}\rho s(\boldsymbol{E}_j(\gamma_{3j})\mathrm{e}^{\gamma_3\rho s}-\boldsymbol{E}_j(-\gamma_{3j})\mathrm{e}^{-\gamma_{3j}\rho s}) & \text{for}\quad \Delta_j=0,\\ \mathrm{e}^{c_{\alpha j}\rho s}\boldsymbol{C}_{\alpha\beta j}(1)+\mathrm{e}^{-c_{\alpha j}\rho s}\boldsymbol{C}_{\alpha\beta j}(-1) & \text{for}\quad \Delta_j<0,\end{cases} \tag{15}$$

where $\boldsymbol{C}_{\alpha\beta j}(\chi)=\boldsymbol{C}_{\alpha j}(\chi)\cos(\chi c_{bj}\rho s)+\boldsymbol{C}_{\beta j}(\chi)\sin(\chi c_{bj}\rho s)$. $\boldsymbol{C}_j(\chi)$, $\boldsymbol{D}_j(\chi)$, $\boldsymbol{E}_j(\chi)$, $\boldsymbol{C}_{\alpha j}(\chi)$, and $\boldsymbol{C}_{\beta j}(\chi)$ are five square coefficient matrices of the five elastic parameters of the jth homogeneous layer ($c_{ij}, i=1,2,\cdots,5;\ j=0,1,\cdots,n+1$). γ_{1j}, γ_{2j}, and γ_{3j} are the roots of the characteristic equations of transversely isotropic elasticity, and c_{aj} and c_{bj} are the material parameters obtained from characteristic roots. The discriminant $\Delta_j=\sqrt{c_{1j}c_{3j}}-c_{2j}-2c_{4j}$. For isotropic materials, $\Delta_j=0$, and $\gamma_{0j}=\gamma_{3j}=1$.

All the coefficient matrices and characteristic roots in Eqs. (13) and (15) are, respectively, given in Appendices A and B.

3 Specific solutions in transform domain

3.1 Boundary and interface conditions

For the regularity condition as the vector $z \to \pm\infty$, the stresses and displacements approach zero. For the perfectly bonded interface connection, the displacement vector $\boldsymbol{u}(x,y,z)$ and the stress vector $\boldsymbol{T}_z(x,y,z)$ are completely continuous at the horizontal interface between any two connected dissimilar elastic layers, i.e.,

$$\lim_{z\to H_j^{\pm}} \boldsymbol{u}(x,y,z) = \boldsymbol{u}(x,y,H_j), \quad \lim_{z\to H_j^{\pm}} \boldsymbol{T}_z(x,y,z) = \boldsymbol{T}_z(x,y,H_j), \quad j=0,1,2,\cdots,n. \tag{16}$$

In the transform domain, using the interface conditions (16), we have

$$\boldsymbol{V}(H_j^-) = \boldsymbol{V}(H_j) = \boldsymbol{V}(H_j^+), \quad \boldsymbol{U}(H_j^-) = \boldsymbol{U}(H_j) = \boldsymbol{U}(H_j^+), \quad j=0,1,2,\cdots,n. \tag{17}$$

3.2 Backward transform matrix method

The general solution matrices in Eqs. (13) and (15) have the functions of exponential growth. These functions can lead to problems in the numerical integration of the inverse Fourier or Hankel integral transforms. They can be eliminated by using the backward transfer matrix method[17]. Appendix C illustrates how to derive the specific solution of $\boldsymbol{V}(z)$ in terms of $\boldsymbol{G}_v$ for $-\infty < z \leqslant d^-$ with the backward transfer matrix method. Similarly, the specific solution of $\boldsymbol{V}(z)$ in terms of $\boldsymbol{G}_v$ for $d^+ \leqslant z < +\infty$ and the specific solution of $\boldsymbol{U}(z)$ in terms of $\boldsymbol{G}_u$ for $-\infty < z \leqslant d^-$ and $d^+ \leqslant z < +\infty$ can be easily obtained. These specific solutions have only the functions of exponential decrease. They are explicitly given below.

3.3 Specific solution of $\boldsymbol{V}(z)$ in terms of $\boldsymbol{G}_v$

The solution of $\boldsymbol{V}(z)$ is expressed as follows:

$$\boldsymbol{V}(z) = \boldsymbol{\Psi}_V(\rho,z)\boldsymbol{G}_v, \tag{18}$$

where $-\infty < z < +\infty$, $0 \leqslant \rho < +\infty$, and $\boldsymbol{\Psi}_V(\rho,z)$ is a square matrix of 2×2 elements.

The 2×2 matrix $\boldsymbol{\Psi}_V(\rho,z)$ in Eq. (18) is a real matrix, and can be explicitly expressed as follows.

(i) For the 0th layer of the upper half-space $-\infty < z \leqslant H_0 \leqslant d^-$,

$$\boldsymbol{\Psi}_V(\rho,z) = \mathrm{e}^{-\gamma_{00}\rho(H_0-z)-\gamma_{01}\rho h_1-\cdots-\gamma_{0(k-1)}\rho h_{k-1}-\gamma_{0k}\rho(d-H_{k-1})}\boldsymbol{B}_0(\gamma_{00})\boldsymbol{N}_{Ap}. \tag{19}$$

(ii) For the jth layer of finite thickness $H_{j-1} \leqslant z \leqslant H_j$ and $z \leqslant d^-$, $j=1,2,\cdots,k-1$, $k\,(\leqslant n)$,

$$\begin{aligned}\boldsymbol{\Psi}_V(\rho,z) =& \,\mathrm{e}^{-\gamma_{0j}\rho(H_j-z)-\gamma_{0(j+1)}\rho h_{j+1}-\cdots-\gamma_{0(k-1)}\rho h_{k-1}-\gamma_{0k}\rho(d-H_{k-1})}\\ &\cdot \boldsymbol{A}_j^p(z-H_{j-1})\boldsymbol{A}_{j-1}^p(h_{j-1})\cdots\boldsymbol{A}_1^p(h_1)\boldsymbol{N}_{Ap},\end{aligned} \tag{20}$$

where the square matrix $\boldsymbol{A}_j^p(s)$ is defined by the following equation:

$$\boldsymbol{A}_j^p(s) = \boldsymbol{B}_j(\gamma_{0j}) + \mathrm{e}^{-2\gamma_{0j}\rho s}\boldsymbol{B}_j(-\gamma_{0j}). \tag{21}$$

(iii) For the jth layer of finite thickness $H_{j-1} \leqslant z \leqslant H_j$ and $z \geqslant d^+$, $j=k,\,k+1,\cdots,n$,

$$\begin{aligned}\boldsymbol{\Psi}_V(\rho,z) =& \,\mathrm{e}^{-\gamma_{0j}\rho(z-H_{j-1})-\gamma_{0(j-1)}\rho h_{j-1}-\cdots-\gamma_{0(k+1)}\rho h_{k+1}-\gamma_{0k}\rho(H_k-d)}\\ &\cdot \boldsymbol{A}_j^q(z-H_j)\boldsymbol{A}_{j+1}^q(-h_{j+1})\cdots\boldsymbol{A}_n^q(-h_n)\boldsymbol{N}_{Aq},\end{aligned} \tag{22}$$

where the square matrix $\boldsymbol{A}_j^q(s)$ is defined by the following equation:

$$\boldsymbol{A}_j^q(s) = \mathrm{e}^{2\gamma_{0j}\rho s}\boldsymbol{B}_j(\gamma_{0j}) + \boldsymbol{B}_j(-\gamma_{0j}). \tag{23}$$

(iv) For the $(n+1)$th layer of the lower half-space $H_n \leqslant z < +\infty$,

$$\boldsymbol{\Psi}_V(\rho,z) = \mathrm{e}^{-\gamma_{0(n+1)}\rho(z-H_n)-\gamma_{0n}\rho h_n-\cdots-\gamma_{0(k+1)}\rho h_{k+1}-\gamma_{0k}\rho(H_k-d)}\boldsymbol{B}_{n+1}(-\gamma_{0(n+1)})\boldsymbol{N}_{Aq}. \tag{24}$$

In Eqs. (19) and (20), the 2×2 matrix $\boldsymbol{N}_{Ap}$ is explicitly expressed as

$$\boldsymbol{N}_{Ap} = \boldsymbol{M}_{Ap}^{-1}\begin{pmatrix} \boldsymbol{0} \\ \boldsymbol{p}_{n+1}\boldsymbol{A}_n^p(h_n)\boldsymbol{A}_{n-1}^p(h_{n-1})\cdots\boldsymbol{A}_{k+1}^p(h_{k+1})\boldsymbol{A}_k^p(H_k-d)\end{pmatrix}, \tag{25}$$

where $\boldsymbol{M}_{Ap}^{-1}$ is the inverse of the 2×2 matrix $\boldsymbol{M}_{Ap}$ defined by

$$\boldsymbol{M}_{Ap} = \begin{pmatrix} \boldsymbol{q}_0 \\ \boldsymbol{p}_{n+1}\boldsymbol{A}_n^p(h_n)\boldsymbol{A}_{n-1}^p(h_{n-1})\cdots\boldsymbol{A}_1^p(h_1)\end{pmatrix}. \tag{26}$$

In Eqs. (22) and (24), the 2×2 matrix $\boldsymbol{N}_{Aq}$ is explicitly expressed as

$$\boldsymbol{N}_{Aq} = -\boldsymbol{M}_{Aq}^{-1}\begin{pmatrix} \boldsymbol{0} \\ \boldsymbol{q}_0\boldsymbol{A}_1^q(-h_1)\boldsymbol{A}_2^q(-h_2)\cdots\boldsymbol{A}_{k-1}^q(-h_{k-1})\boldsymbol{A}_k^q(H_{k-1}-d)\end{pmatrix}, \tag{27}$$

where $\boldsymbol{M}_{Aq}^{-1}$ is the inverse of the 2×2 matrix $\boldsymbol{M}_{Aq}$ defined by

$$\boldsymbol{M}_{Aq} = \begin{pmatrix} \boldsymbol{p}_{n+1} \\ \boldsymbol{q}_0\boldsymbol{A}_1^q(-h_1)\boldsymbol{A}_2^q(-h_2)\cdots\boldsymbol{A}_n^q(-h_n)\end{pmatrix}. \tag{28}$$

In the above equations, the material matrices $\boldsymbol{q}_0$ and $\boldsymbol{p}_{n+1}$ are given in Appendix A.

3.4 Specific solution of $\boldsymbol{U}(z)$ in terms of $\boldsymbol{G_u}$

The solution of $\boldsymbol{U}(z)$ is expressed as follows:

$$\boldsymbol{U}(z) = \boldsymbol{\Psi}_U(\rho,z)\boldsymbol{G}_u, \tag{29}$$

where $-\infty < z < +\infty$, $0 \leqslant \rho < +\infty$, and $\boldsymbol{\Psi}_U(\rho,z)$ is a square matrix of 4×4 elements.

The 4×4 matrix $\boldsymbol{\Psi}_U(\rho,z)$ in Eq. (29) is a real matrix, and can be explicitly expressed as follows.

(i) For the 0th layer of the upper half-space $-\infty < z \leqslant H_0$,

$$\boldsymbol{\Psi}_U(\rho,z) = \mathrm{e}^{-\gamma_{a1}\rho h_1-\cdots-\gamma_{a(k-1)}\rho h_{(k-1)}-\gamma_{ak}\rho(d-H_{k-1})}\boldsymbol{Q}_0^p(H_0-z)\boldsymbol{N}_{Qp}, \tag{30a}$$

where $\gamma_{aj} = \gamma_{1j}$ for $\Delta_j > 0$, $\gamma_{aj} = \gamma_{3j}$ for $\Delta_j = 0$, and $\gamma_{aj} = c_{aj}$ for $\Delta_j < 0$ $(j = 1,2,\cdots, k-1,k)$. The 4×4 matrix $\boldsymbol{Q}_0^p(s)$ is defined by the following equations:

$$\boldsymbol{Q}_0^p(s) = \begin{cases} \mathrm{e}^{-\gamma_{10}\rho s}\boldsymbol{C}_0(\gamma_{10}) - \mathrm{e}^{-\gamma_{20}\rho s}\boldsymbol{C}_0(\gamma_{20}) & \text{for} \quad \Delta_0 > 0, \\ \mathrm{e}^{-\gamma_{30}\rho s}(\boldsymbol{D}_0(\gamma_{30}) - \gamma_{30}\rho s\boldsymbol{E}_0(\gamma_{30})) & \text{for} \quad \Delta_0 = 0, \\ \mathrm{e}^{-c_{a0}\rho s}\boldsymbol{C}_{\alpha\beta 0}(1) & \text{for} \quad \Delta_0 < 0. \end{cases} \tag{30b}$$

(ii) For the jth layer of finite thickness $H_{j-1} \leqslant z \leqslant H_j$ and $z \leqslant d^-$, $j = 1,2,\cdots,k-1$, $k\,(\leqslant n)$,

$$\begin{aligned}\boldsymbol{\Psi}_U(\rho,z) = {} & \mathrm{e}^{-\gamma_{aj}\rho(H_j-z)-\gamma_{a(j+1)}\rho h_{j+1}-\cdots-\gamma_{a(k-1)}\rho h_{k-1}-\gamma_{ak}\rho(d-H_{k-1})} \\ & \cdot\boldsymbol{Q}_j^p(z-H_{j-1})\boldsymbol{Q}_{j-1}^p(h_{j-1})\cdots\boldsymbol{Q}_1^p(h_1)\boldsymbol{N}_{Qp},\end{aligned} \tag{31}$$

where $\gamma_{aj}=\gamma_{1j}$ for $\Delta_j>0$, $\gamma_{aj}=\gamma_{3j}$ for $\Delta_j=0$, and $\gamma_{aj}=c_{aj}$ for $\Delta_j<0$. The 4×4 matrix $\boldsymbol{Q}_j^p(s)$ is defined by the following equations:

$$\boldsymbol{Q}_j^p(s)=\begin{cases}\boldsymbol{C}_j(\gamma_{1j})-\mathrm{e}^{-(\gamma_{1j}-\gamma_{2j})\rho s}\boldsymbol{C}_j(\gamma_{2j})+\mathrm{e}^{-2\gamma_{1}\rho s}\boldsymbol{C}_j(-\gamma_{1j})\\ \quad-\mathrm{e}^{-(\gamma_{1j}+\gamma_{2j})\rho s}\boldsymbol{C}_j(-\gamma_{2j})\quad\text{for}\quad\Delta_j>0,\\ \boldsymbol{D}_j(\gamma_{3j})+\gamma_{3j}\rho s\boldsymbol{E}_j(\gamma_{3j})+\mathrm{e}^{-2\gamma_{3j}\rho s}(\boldsymbol{D}_j(-\gamma_{3j})-\gamma_{3j}\rho s\boldsymbol{E}_j(-\gamma_{3j}))\quad\text{for}\quad\Delta_j=0,\\ \boldsymbol{C}_{\alpha\beta j}(1)+\mathrm{e}^{-2c_a\rho s}\boldsymbol{C}_{\alpha\beta j}(-1)\quad\text{for}\quad\Delta_j<0.\end{cases}\tag{32}$$

(iii) For the jth layer of finite thickness $H_{j-1}\leqslant z\leqslant H_j$ and $z\geqslant d^+$, $j=k,\,k+1,\cdots,n$,

$$\begin{aligned}\boldsymbol{\Psi}_U(\rho,z)=&\,\mathrm{e}^{-\gamma_{aj}\rho(z-H_{j-1})-\gamma_{a(j-1)}\rho h_{j-1}-\cdots-\gamma_{a(k+1)}\rho h_{k+1}-\gamma_{ak}\rho(H_k-d)}\\&\cdot\boldsymbol{Q}_j^q(z-H_j)\boldsymbol{Q}_{j+1}^q(-h_{j+1})\cdots\boldsymbol{Q}_n^q(-h_n)\boldsymbol{N}_{Qq},\end{aligned}\tag{33}$$

where $\gamma_{aj}=\gamma_{1j}$ for $\Delta_j>0$, $\gamma_{aj}=\gamma_{3j}$ for $\Delta_j=0$, and $\gamma_{aj}=c_{aj}$ for $\Delta_j<0$. The 4×4 matrix $\boldsymbol{Q}_j^q(s)$ is defined as

$$\boldsymbol{Q}_j^q(s)=\begin{cases}\mathrm{e}^{2\gamma_{1j}\rho s}\boldsymbol{C}_j(\gamma_{1j})-\mathrm{e}^{(\gamma_{1j}+\gamma_{2j})\rho s}\boldsymbol{C}_j(\gamma_{2j})+\boldsymbol{C}_j(-\gamma_{1j})\\ \quad-\mathrm{e}^{(\gamma_{1j}-\gamma_{2j})\rho s}\boldsymbol{C}_j(-\gamma_{2j})\quad\text{for}\quad\Delta_j>0,\\ \mathrm{e}^{2\gamma_{3j}\rho s}(\boldsymbol{D}_j(\gamma_{3j})+\gamma_{3j}\rho s\boldsymbol{E}_j(\gamma_{3j}))+\boldsymbol{D}_j(-\gamma_{3j})\\ \quad-\gamma_{3j}\rho s\boldsymbol{E}_j(-\gamma_{3j})\quad\text{for}\quad\Delta_j=0,\\ \mathrm{e}^{2c_{aj}\rho s}\boldsymbol{C}_{\alpha\beta j}(1)+\boldsymbol{C}_{\alpha\beta j}(-1)\quad\text{for}\quad\Delta_j<0.\end{cases}\tag{34}$$

(iv) For the $(n+1)$th layer of the lower half-space $H_n\leqslant z<+\infty$,

$$\boldsymbol{\Psi}_U(\rho,z)=\mathrm{e}^{-\gamma_{an}\rho h_n-\gamma_{a(n-1)}\rho h_{n-1}-\cdots-\gamma_{a(k+1)}\rho h_{k+1}-\gamma_{ak}\rho(H_k-d)}\boldsymbol{Q}_{(n+1)}^q(z-H_n)\boldsymbol{N}_{Qq},\tag{35a}$$

where $\gamma_{aj}=\gamma_{1j}$ for $\Delta_j>0$, $\gamma_{aj}=\gamma_{3j}$ for $\Delta_j=0$, and $\gamma_{aj}=c_{aj}$ for $\Delta_j<0\,(j=k,k+1,\cdots,n)$. The 4×4 matrix $\boldsymbol{Q}_{(n+1)}^q(s)$ is defined as

$$\begin{aligned}&\boldsymbol{Q}_{(n+1)}^q(s)\\&=\begin{cases}\mathrm{e}^{-\gamma_{1(n+1)}\rho s}\boldsymbol{C}_{n+1}(-\gamma_{1(n+1)})-\mathrm{e}^{-\gamma_{2(n+1)}\rho s}\boldsymbol{C}_{n+1}(-\gamma_{2(n+1)})\quad\text{for}\quad\Delta_{(n+1)}>0,\\ \mathrm{e}^{-\gamma_{3(n+1)}\rho s}(\boldsymbol{D}_{n+1}(-\gamma_{3(n+1)})-\gamma_{3(n+1)}\rho s\boldsymbol{E}_{n+1}(-\gamma_{3(n+1)}))\quad\text{for}\quad\Delta_{(n+1)}=0,\\ \mathrm{e}^{-c_{a(n+1)}\rho s}\boldsymbol{C}_{\alpha\beta(n+1)}(-1)\quad\text{for}\quad\Delta_{(n+1)}<0.\end{cases}\end{aligned}\tag{35b}$$

In Eqs. (30) and (31), the 4×4 matrix $\boldsymbol{N}_{Qp}$ is explicitly expressed as

$$\boldsymbol{N}_{Qp}=\boldsymbol{M}_{Qp}^{-1}\begin{pmatrix}\boldsymbol{0}\\ \boldsymbol{p}_{p(n+1)}\boldsymbol{Q}_n^p(h_n)\boldsymbol{Q}_{n-1}^p(h_{n-1})\cdots\boldsymbol{Q}_{k+1}^p(h_{k+1})\boldsymbol{Q}_k^p(H_k-d)\end{pmatrix},\tag{36}$$

where $\boldsymbol{M}_{Qp}^{-1}$ is the inverse of the 4×4 matrix $\boldsymbol{M}_{Qp}$ defined by

$$\boldsymbol{M}_{Qp}=\begin{pmatrix}\boldsymbol{P}_{q0}\\ \boldsymbol{P}_{p(n+1)}\boldsymbol{Q}_n^p(h_n)\boldsymbol{Q}_{n-1}^p(h_{n-1})\cdots\boldsymbol{Q}_1^p(h_1)\end{pmatrix}.\tag{37}$$

In Eqs. (33) and (35), the 4×4 matrix $\boldsymbol{N}_{Qq}$ is defined by

$$\boldsymbol{N}_{Qq}=-\boldsymbol{M}_{Qq}^{-1}\begin{pmatrix}\boldsymbol{0}\\ \boldsymbol{P}_{q0}\boldsymbol{Q}_1^q(-h_1)\boldsymbol{Q}_2^q(-h_2)\cdots\boldsymbol{Q}_{k-1}^q(-h_{k-1})\boldsymbol{Q}_k^q(H_{k-1}-d)\end{pmatrix},\tag{38}$$

where $\boldsymbol{M}_{Qq}^{-1}$ is the inverse of the 4×4 matrix $\boldsymbol{M}_{Qq}$ defined by

$$\boldsymbol{M}_{Qq}=\begin{pmatrix}\boldsymbol{P}_{p(n+1)}\\ \boldsymbol{P}_{q0}\boldsymbol{Q}_1^q(-h_1)\boldsymbol{Q}_2^q(-h_2)\cdots\boldsymbol{Q}_n^p(-h_n)\end{pmatrix}. \tag{39}$$

In the above equations, the material matrices $\boldsymbol{P}_{q0}$ and $\boldsymbol{P}_{p(n+1)}$ are given in Appendix A.

3.5 Specific solutions of $\boldsymbol{w}(z)$ and $\boldsymbol{Y}_z(z)$ in terms of $\boldsymbol{g}(\xi,\eta)$

The specific solutions of $\boldsymbol{V}(z)$ and $\boldsymbol{U}(z)$ are given in Eqs. (18) and (29) in terms of the two loading matrices $\boldsymbol{G}_v(\xi,\eta)$ and $\boldsymbol{G}_u(\xi,\eta)$. $\boldsymbol{V}(z)$ and $\boldsymbol{U}(z)$ can be expressed as follows:

$$\boldsymbol{V}(z)=\begin{pmatrix}w_2\\ \tau_2\end{pmatrix}=\begin{pmatrix}\Phi_{bb}(\rho,z) & \Phi_{22}(\rho,z)\\ \Psi_{bb}(\rho,z) & \Psi_{22}(\rho,z)\end{pmatrix}\begin{pmatrix}0\\ g_2\end{pmatrix}, \tag{40}$$

$$\boldsymbol{U}(z)=\begin{pmatrix}w_1\\ w_3\\ \tau_3\\ \tau_1\end{pmatrix}=\begin{pmatrix}\Phi_{ac}(\rho,z) & \Phi_{aa}(\rho,z) & \Phi_{13}(\rho,z) & \Phi_{11}(\rho,z)\\ \Phi_{cc}(\rho,z) & \Phi_{ca}(\rho,z) & \Phi_{33}(\rho,z) & \Phi_{31}(\rho,z)\\ \Psi_{cc}(\rho,z) & \Psi_{ca}(\rho,z) & \Psi_{33}(\rho,z) & \Psi_{31}(\rho,z)\\ \Psi_{ac}(\rho,z) & \Psi_{aa}(\rho,z) & \Psi_{13}(\rho,z) & \Psi_{11}(\rho,z)\end{pmatrix}\begin{pmatrix}0\\ 0\\ g_3\\ g_1\end{pmatrix}. \tag{41}$$

As a result, the solutions of $\boldsymbol{w}(z)$ and $\boldsymbol{Y}_z(z)$ can be expressed as follows in terms of the body force loading vector $\boldsymbol{g}(\xi,\eta)$:

$$\boldsymbol{w}(\xi,\eta,z)=\boldsymbol{\Phi}(\rho,z)\boldsymbol{g}(\xi,\eta),\quad \boldsymbol{Y}_z(\xi,\eta,z)=\boldsymbol{\Psi}(\rho,z)\boldsymbol{g}(\xi,\eta), \tag{42}$$

where

$$\begin{cases}\boldsymbol{\Phi}(\rho,z)=\begin{pmatrix}\Phi_{11}(\rho,z) & 0 & \Phi_{13}(\rho,z)\\ 0 & \Phi_{22}(\rho,z) & 0\\ \Phi_{31}(\rho,z) & 0 & \Phi_{33}(\rho,z)\end{pmatrix},\\ \boldsymbol{\Psi}(\rho,z)=\begin{pmatrix}\Psi_{11}(\rho,z) & 0 & \Psi_{13}(\rho,z)\\ 0 & \Psi_{22}(\rho,z) & 0\\ \Psi_{31}(\rho,z) & 0 & \Psi_{33}(\rho,z)\end{pmatrix}.\end{cases} \tag{43}$$

4 Specific solutions in physical domain

4.1 Specific solutions in inverse double Fourier transform integrals

Using Eqs. (7), (9), (10), and (43), the solutions of the field variable vectors $\boldsymbol{u}(x,y,z)$, $\boldsymbol{T}_z(x,y,z)$, and $\boldsymbol{\Gamma}_{\mathrm{p}}(x,y,z)$ in the FGM model ($-\infty<x,y,z<+\infty$) due to the internal loading $\boldsymbol{f}(x,y)$ concentrated on a horizontal plane, i.e., $\boldsymbol{f}(x,y,z)=\boldsymbol{f}(x,y)\delta(z-d)$, can be expressed as follows:

$$\begin{cases}\boldsymbol{u}(x,y,z)=\dfrac{1}{2\pi}\displaystyle\int_{-\infty}^{+\infty}\int_{-\infty}^{+\infty}\frac{1}{\rho}\boldsymbol{\Pi}\boldsymbol{\Phi}(\rho,z)\boldsymbol{\Pi}^*\widetilde{\boldsymbol{f}}(\xi,\eta)K\mathrm{d}\xi\mathrm{d}\eta,\\ \boldsymbol{T}_z(x,y,z)=\dfrac{1}{2\pi}\displaystyle\int_{-\infty}^{+\infty}\int_{-\infty}^{+\infty}\boldsymbol{\Pi}\boldsymbol{\Psi}(\rho,z)\boldsymbol{\Pi}^*\widetilde{\boldsymbol{f}}(\xi,\eta)K\mathrm{d}\xi\mathrm{d}\eta,\\ \boldsymbol{\Gamma}_{\mathrm{p}}(x,y,z)=\dfrac{1}{2\pi}\displaystyle\int_{-\infty}^{+\infty}\int_{-\infty}^{+\infty}\boldsymbol{\Pi}_{\mathrm{p}}\boldsymbol{\Phi}(\rho,z)\boldsymbol{\Pi}^*\widetilde{\boldsymbol{f}}(\xi,\eta)K\mathrm{d}\xi\mathrm{d}\eta,\end{cases} \tag{44}$$

where the body force vector $\widetilde{\boldsymbol{f}}(\xi,\eta)$ in the transform domain is expressed as follows:

$$\widetilde{\boldsymbol{f}}(\xi,\eta)=\frac{1}{2\pi}\int_{-\infty}^{+\infty}\int_{-\infty}^{+\infty}\boldsymbol{f}(x,y)K^*\mathrm{d}x\mathrm{d}y. \tag{45}$$

4.2 Specific solutions for point force vector

The fundamental singular solution due to the body force vector $\boldsymbol{f}(x,y)$ concentrated at the point $(0,0,d)$ can be expressed as follows:

$$\boldsymbol{f}(x,y)=\delta(x)\delta(y)\boldsymbol{f}_{\rm c},\quad \widetilde{\boldsymbol{f}}(\xi,\eta)=\frac{\boldsymbol{f}_{\rm c}}{2\pi}. \tag{46}$$

Consequently, the displacements $\boldsymbol{u}$, the vertical stresses $\boldsymbol{T}_z$, and the plane strains $\boldsymbol{\Gamma}_{\rm p}$ can be expressed as

$$\boldsymbol{u}(x,y,z)=\boldsymbol{G}_u(x,y,z)\boldsymbol{f}_{\rm c},\quad \boldsymbol{T}_z(x,y,z)=\boldsymbol{G}_z(x,y,z)\boldsymbol{f}_{\rm c},\quad \boldsymbol{\Gamma}_{\rm p}(x,y,z)=\boldsymbol{G}_{\rm p}(x,y,z)\boldsymbol{f}_{\rm c}, \tag{47}$$

where Green's functions are

$$\begin{cases} 2\pi\boldsymbol{G}_u(x,y,z)=\dfrac{1}{2\pi}\displaystyle\int_{-\infty}^{+\infty}\int_{-\infty}^{+\infty}\frac{1}{\rho}\boldsymbol{\Pi}\boldsymbol{\Phi}(\rho,z)\boldsymbol{\Pi}^*K{\rm d}\xi{\rm d}\eta, \\ 2\pi\boldsymbol{G}_z(x,y,z)=\dfrac{1}{2\pi}\displaystyle\int_{-\infty}^{+\infty}\int_{-\infty}^{+\infty}\boldsymbol{\Pi}\boldsymbol{\Psi}(\rho,z)\boldsymbol{\Pi}^*K{\rm d}\xi{\rm d}\eta, \\ 2\pi\boldsymbol{G}_{\rm p}(x,y,z)=\dfrac{1}{2\pi}\displaystyle\int_{-\infty}^{+\infty}\int_{-\infty}^{+\infty}\boldsymbol{\Pi}_{\rm p}\boldsymbol{\Phi}(\rho,z)\boldsymbol{\Pi}^*K{\rm d}\xi{\rm d}\eta. \end{cases} \tag{48}$$

The relationships of the independent variables between the Cartesian and cylindrical coordinates in the physical domain can be defined as follows:

$$x=r\cos\theta,\quad y=r\sin\theta,\quad z=z,\quad r=\sqrt{x^2+y^2}. \tag{49}$$

Similarly, the relationships of the independent variables between the Cartesian and cylindrical coordinates in the transform domain can be defined as follows:

$$\xi=\rho\sin\varphi,\quad \eta=\rho\cos\varphi,\quad z=z,\quad \rho=\sqrt{\xi^2+\eta^2}. \tag{50}$$

The identity of Bessel functions of order m can be expressed as follows:

$$\mathrm{J}_m=\mathrm{J}_m(\rho r)=\frac{1}{2\pi}\int_0^{2\pi}{\rm e}^{\pm{\rm i}(\rho r\sin\theta-m\theta)}{\rm d}\theta,\quad m=0,\pm1,\pm2,\pm3,\cdots. \tag{51}$$

Consequently, Green's functions in Eq. (48) can be simplified as the following Hankel transform integrals with the semi-infinite interval from 0 to $+\infty$, i.e.,

$$2\pi\boldsymbol{G}_u(x,y,z)=\int_0^{+\infty}\begin{pmatrix} \Phi_1\mathrm{J}_0-\dfrac{x^2-y^2}{r^2}\Phi_2\mathrm{J}_2 & -\dfrac{2xy}{r^2}\Phi_2\mathrm{J}_2 & -\dfrac{x}{r}\Phi_{13}\mathrm{J}_1 \\ -\dfrac{2xy}{r^2}\Phi_2\mathrm{J}_2 & \Phi_1\mathrm{J}_0+\dfrac{x^2-y^2}{r^2}\Phi_2\mathrm{J}_2 & -\dfrac{y}{r}\Phi_{13}\mathrm{J}_1 \\ \dfrac{x}{r}\Phi_{31}\mathrm{J}_1 & \dfrac{y}{r}\Phi_{31}\mathrm{J}_1 & \Phi_{33}\mathrm{J}_0 \end{pmatrix}{\rm d}\rho, \tag{52a}$$

$$2\pi\boldsymbol{G}_z(x,y,z)=\int_0^{+\infty}\begin{pmatrix} \Psi_1\mathrm{J}_0-\dfrac{x^2-y^2}{r^2}\Psi_2\mathrm{J}_2 & -\dfrac{2xy}{r^2}\Psi_2\mathrm{J}_2 & -\dfrac{x}{r}\Psi_{13}\mathrm{J}_1 \\ -\dfrac{2xy}{r^2}\Psi_2\mathrm{J}_2 & \Psi_1\mathrm{J}_0+\dfrac{x^2-y^2}{r^2}\Psi_2\mathrm{J}_2 & -\dfrac{y}{r}\Psi_{13}\mathrm{J}_1 \\ \dfrac{x}{r}\Psi_{31}\mathrm{J}_1 & \dfrac{y}{r}\Psi_{31}\mathrm{J}_1 & \Psi_{33}\mathrm{J}_0 \end{pmatrix}\rho{\rm d}\rho, \tag{52b}$$

$$2\pi\boldsymbol{G}_{\mathrm{p}}(x,y,z)=-\frac{1}{2}\int_0^{+\infty}\begin{pmatrix}\frac{x}{r}(2\Phi_1+\Phi_2)\mathrm{J}_1 & \frac{y}{r}\Phi_2\mathrm{J}_1 & \Phi_{13}\mathrm{J}_0\\ \frac{y}{r}\Phi_1\mathrm{J}_1 & \frac{x}{r}\Phi_1\mathrm{J}_1 & 0\\ \frac{x}{r}\Phi_2\mathrm{J}_1 & \frac{y}{r}(2\Phi_1+\Phi_2)\mathrm{J}_1 & \Phi_{13}\mathrm{J}_0\end{pmatrix}\rho\mathrm{d}\rho$$
$$+\frac{1}{2}\int_0^{+\infty}\begin{pmatrix}\left(\frac{4x^3}{r^3}-\frac{3x}{r}\right)\Phi_2\mathrm{J}_3 & \left(\frac{3y}{r}-\frac{4y^3}{r^3}\right)\Phi_2\mathrm{J}_3 & \frac{x^2-y^2}{r^2}\Phi_{13}\mathrm{J}_2\\ \left(\frac{3y}{r}-\frac{4y^3}{r^3}\right)\Phi_2\mathrm{J}_3 & \left(\frac{3x}{r}-\frac{4x^3}{r^3}\right)\Phi_2\mathrm{J}_3 & \frac{2xy}{r^2}\Phi_{13}\mathrm{J}_2\\ \left(\frac{3x}{r}-\frac{4x^3}{r^3}\right)\Phi_2\mathrm{J}_3 & \left(\frac{4y^3}{r^3}-\frac{3y}{r}\right)\Phi_2\mathrm{J}_3 & \frac{y^2-x^2}{r^2}\Phi_{13}\mathrm{J}_2\end{pmatrix}\rho\mathrm{d}\rho, \quad (52c)$$

where

$$\Phi_1=\frac{1}{2}(\Phi_{11}+\Phi_{22}),\quad \Phi_2=\frac{1}{2}(\Phi_{11}-\Phi_{22}),$$
$$\Psi_1=\frac{1}{2}(\Psi_{11}+\Psi_{22}),\quad \Psi_2=\frac{1}{2}(\Psi_{11}-\Psi_{22}).$$

Φ_{11}, Φ_{13}, Φ_{22}, Φ_{31}, Φ_{33}, Ψ_{11}, Ψ_{13}, Ψ_{22}, Ψ_{31}, and Ψ_{33} are ten kernel functions associated with the n-layered FGM model and given in Section 3.

5 Isolation of singular terms and precise computation of complete solutions

5.1 Properties of ten kernel functions

The specific solutions of $\boldsymbol{\Phi}(\rho,z)$ and $\boldsymbol{\Psi}(\rho,z)$ depend on the material parameters, the interface conditions, and the location of the loading plane $z=d$. They are independent of the specific loading conditions on the loading plane ($z=d$). All the components of the 3×3 matrices $\boldsymbol{\Phi}(\rho,z)$ and $\boldsymbol{\Psi}(\rho,z)$ in Eq. (43) are real values and free of any functions of exponential growth with ρ. The solutions in Eq. (52) are expressed in terms of the improper Hankel transform integrals with semi-infinity extent, and their integral variable ρ has to approach infinity ($+\infty$) during integration. If $\boldsymbol{\Phi}(\rho,z)$ and $\boldsymbol{\Psi}(\rho,z)$ have any functions of exponential growth with ρ, these integrations would be problematic and ill-conditioned, and can cause numerical overflow and instability. The backward transfer matrix method eliminates all the functions of exponential growth $\mathrm{e}^{|\gamma|\rho|z|}(0\leqslant\rho<+\infty)$, and keeps only the functions of exponential decrease $\mathrm{e}^{-|\gamma|\rho|z|}$ during the exact and explicit formulation. Note that $\gamma=\min(\gamma_{1j},\gamma_{2j})$ for $\Delta_j>0$, $\gamma=\min(\gamma_{3j})$ for $\Delta_j=0$, and $\gamma=\min(c_{aj})$ for $\Delta_j<0$, where $j=0,1,2,\cdots,n+1$. As a result, $\boldsymbol{\Phi}(\rho,z)$ and $\boldsymbol{\Psi}(\rho,z)$ rapidly tend to zero or constant values as ρ becomes larger and larger, which ensures the numerical precision, convergence, and stability of the solutions in the matrix forms of the Hankel transform integrals in Eq. (52).

5.2 Asymptotic expression of ten kernel functions as ρ approaches $+\infty$

$\boldsymbol{\Phi}(\rho,z)$ and $\boldsymbol{\Psi}(\rho,z)$ have no singular poles for $0\leqslant\rho<+\infty$, and have the exact asymptotic expressions for $\rho\to+\infty$. If the depth z is not located at or closely adjacent to the loading plane ($z=d$), $\boldsymbol{\Phi}(\rho,z)$ and $\boldsymbol{\Psi}(\rho,z)$ rapidly decrease to zero following the functions of exponential decrease (i.e., $\mathrm{e}^{-|\gamma|\rho|z-d|}$) as $\rho\to+\infty$. If the depth z approaches the loading plane (i.e., $|z-d|\leqslant\delta_{\mathrm{a}}$), where δ_{a} is an arbitrary positive value less than the thicknesses of the two homogeneous layers adjacent to the loading plane $z=d$, the functions of exponential decrease (i.e., $\mathrm{e}^{-|\gamma|\rho|z-d|}$) become slow and slow as $\rho\to+\infty$. They are equal to one at $z=d$. The Hankel transform integrals in Eq. (52) become improper and convergent under the sense of the Cauchy principle value.

We have shown that $\boldsymbol{\Phi}(\rho,z)$ and $\boldsymbol{\Psi}(\rho,z)$ have the following asymptotic expressions as $|\gamma|\rho\delta_{\rm a}\to+\infty$:

$$\lim_{|z-d|\to 0}\boldsymbol{\Phi}(\rho,z)\approx\boldsymbol{\Phi}^{\rm two}(\rho,z),\quad \lim_{|z-d|\to 0}\boldsymbol{\Psi}(\rho,z)\approx\boldsymbol{\Psi}^{\rm two}(\rho,z),\tag{53}$$

where $\boldsymbol{\Phi}^{\rm two}(\rho,z)$ and $\boldsymbol{\Psi}^{\rm two}(\rho,z)$ are the two 3×3 kernel matrices associated with the point load solutions for the case of the bi-material full-space with the material parameters of the two adjacent layers $(c_{i(k-1)},c_{ik})$ or $(c_{ik},c_{i(k+1)})$ surrounding the loading plane $d\,(H_{k-1}\leqslant d\leqslant H_k)$ of $\boldsymbol{f}=\boldsymbol{f}_{\rm c}\delta(x)\delta(y)\delta(z-d)$.

5.3 Isolation of singular terms in the point load solutions

Due to the presence of the weak convergence of the Hankel transform integrals in the sense of Cauchy principal value, the point load solutions in Eq. (6) have to be re-expressed as follows:

$$\begin{cases}\boldsymbol{u}(x,y,z,d)=\boldsymbol{G}_u(x,y,z,\boldsymbol{\Phi}^{\#})\boldsymbol{f}_{\rm c}+\boldsymbol{u}^{\text{two-upper}}(x,y,z,d)\\ \qquad\qquad+\boldsymbol{u}^{\text{two-lower}}(x,y,z,d)-\boldsymbol{u}^{\rm one}(x,y,z,d),\\ \boldsymbol{T}_z(x,y,z,d)=\boldsymbol{G}_z(x,y,z,\boldsymbol{\Psi}^{\#})\boldsymbol{f}_{\rm c}+\boldsymbol{T}_z^{\text{two-upper}}(x,y,z,d)\\ \qquad\qquad+\boldsymbol{T}_z^{\text{two-lower}}(x,y,z,d)-\boldsymbol{T}_z^{\rm one}(x,y,z,d),\\ \boldsymbol{\Gamma}_{\rm p}(x,y,z,d)=\boldsymbol{G}_{\rm p}(x,y,z,\boldsymbol{\Phi}^{\#})\boldsymbol{f}_{\rm c}+\boldsymbol{\Gamma}_{\rm p}^{\text{two-upper}}(x,y,z,d)\\ \qquad\qquad+\boldsymbol{\Gamma}_{\rm p}^{\text{two-lower}}(x,y,z,d)-\boldsymbol{\Gamma}_{\rm p}^{\rm one}(x,y,z,d),\end{cases}\tag{54}$$

where $-\infty<x,y,z<+\infty$, and $H_{k-1}\leqslant d<H_k$.

In Eq. (54), the superscript two-upper denotes the upper bi-material full-space formed with the two sets of the elastic parameters of the $(k-1)$th layer and the kth layer. The superscript two-lower denotes the lower bi-material full-space formed with the two sets of the elastic parameters of the kth layer and the $(k+1)$th layer. The superscript one denotes the homogeneous full-space formed with the one set of the elastic parameters of the kth layer. $\boldsymbol{u}^{\text{two-upper}}$, $\boldsymbol{T}_z^{\text{two-upper}}$, and $\boldsymbol{\Gamma}_{\rm p}^{\text{two-upper}}$ are, respectively, the displacements, the vertical stresses, and the plane strains for the upper bi-material full-space induced by the point load vector in the lower half-space. $\boldsymbol{u}^{\text{two-lower}}$, $\boldsymbol{T}_z^{\text{two-lower}}$, and $\boldsymbol{\Gamma}_{\rm p}^{\text{two-lower}}$ are, respectively, the displacements, vertical stresses, and plane strains for the lower bi-material full-space induced by the point load vector in the upper half-space. $\boldsymbol{u}^{\rm one}$, $\boldsymbol{T}_z^{\rm one}$, and $\boldsymbol{\Gamma}_{\rm p}^{\rm one}$ are, respectively, the displacements, vertical stresses, and plane strains for the homogeneous full-space induced by the point load vector. These complete point load solutions in exact closed forms are given by Yue[12].

In Eq. (54), the two remaining kernel matrices $\boldsymbol{\Phi}^{\#}$ and $\boldsymbol{\Psi}^{\#}$ are expressed as

$$\begin{cases}\boldsymbol{\Phi}^{\#}(\rho,z,d)=\boldsymbol{\Phi}(\rho,z,d)-\boldsymbol{\Phi}^{\text{two-upper}}(\rho,z,d)-\boldsymbol{\Phi}^{\text{two-lower}}(\rho,z,d)+\boldsymbol{\Phi}^{\rm one}(\rho,z,d),\\ \boldsymbol{\Psi}^{\#}(\rho,z,d)=\boldsymbol{\Psi}(\rho,z,d)-\boldsymbol{\Psi}^{\text{two-upper}}(\rho,z,d)-\boldsymbol{\Psi}^{\text{two-lower}}(\rho,z,d)+\boldsymbol{\Psi}^{\rm one}(\rho,z,d),\end{cases}\tag{55}$$

where $\boldsymbol{\Phi}$ and $\boldsymbol{\Psi}$ are the two kernel matrices for an n-layered model in Eq. (43), $\boldsymbol{\Phi}^{\text{two-upper}}$ and $\boldsymbol{\Psi}^{\text{two-upper}}$ are the two kernel matrices for the upper bi-material full-space, $\boldsymbol{\Phi}^{\text{two-lower}}$ and $\boldsymbol{\Psi}^{\text{two-lower}}$ are the two kernel matrices for the lower bi-material full-space, and $\boldsymbol{\Phi}^{\rm one}$ and $\boldsymbol{\Psi}^{\rm one}$ are the two kernel matrices for the homogeneous full-space. These particular kernel matrices are explicitly given by Yue[12].

5.4 Numerical integrations with controlled precision

According to Eq. (54), only the first terms, i.e., $\boldsymbol{G}_u(x,y,z,\boldsymbol{\Phi}^{\#})$, $\boldsymbol{G}_z(x,y,z,\boldsymbol{\Psi}^{\#})$, and $\boldsymbol{G}_{\rm p}(x,y,z,\boldsymbol{\Phi}^{\#})$, need to be numerically calculated. Each of the fifteen improper integrals in

Eq. (53) with ten remaining kernel functions can be further expressed as follows:

$$\int_0^{+\infty} \Phi_{33}^{\#}(\rho,z,d)\mathrm{J}_0(\rho r)\mathrm{d}\rho \approx \int_0^{A_1} \Phi_{33}^{\#}(\rho,z,d)\mathrm{J}_0(\rho r)\mathrm{d}\rho + \cdots + \int_{A_m}^{A_{m+1}} \Phi_{33}^{\#}(\rho,z,d)\mathrm{J}_0(\rho r)\mathrm{d}\rho. \tag{56}$$

Each finite integral on the right-hand side of Eq. (56) is a proper integral, and can be calculated by using Simpson's quadrature based on adaptively iterative integrations with an assigned absolute or relative error δ_{c}. The limits of $A_1, A_2, \cdots, A_m, A_{m+1}$ are chosen according to the rule $A_l = \lambda A_{l-1}$, where $l = 2, 3, \cdots, m, m+1$. In particular, $A_1 = 2$ and $\lambda = 1.5$ are adopted in the computer programming. The evaluation of the finite integrals of these fifteen semi-infinite integrals is automatically terminated provided that the following criterion is satisfied:

$$\frac{|\int_{A_m}^{A_{m+1}} \Phi_A^{\#}(\rho,z,d)\mathrm{J}_B(\rho r)\rho^{0 \text{ or } 1}\mathrm{d}\rho|}{1+\sum\limits_{i=1}^{m}(|\int_{A_i}^{A_{i+1}} \Phi_A^{\#}(\rho,z,d)\mathrm{J}_B(\rho r)\rho^{0 \text{ or } 1}\mathrm{d}\rho|)} \leqslant \delta_{\mathrm{c}}, \tag{57}$$

where $\Phi_A^{\#}$ is one of the ten remaining kernel functions, and $\mathrm{J}_B(\rho r)$ is the corresponding Bessel function of the order 0, 1, 2, or 3.

6 Numerical results and analyses of case study

This section presents a case study to explore the behavior of the n-layered FGM model (see Table 1) subject to point loads, and shows the wide applicability of the point load solutions. This FGM model is also used to calculate the elastic fields induced by circular ring force vectors[26].

Table 1 Five elastic parameters of transversely isotropic FGM model for case study

Layer number	$\overline{z}(=z/h)$	$E_x(z)$/GPa	$\nu_{xy}(z)$	$\frac{E_x}{E_z}$	$\frac{\nu_{xy}}{\nu_{xz}}$	$\frac{\mu_{xy}}{\mu_{xz}}$	Δ
0	$\overline{z}<0$	269.84	0.221 4	0.75	1	1	>0
1	$0\leqslant\overline{z}<0.245\,15$	$225+42.01\overline{z}^{0.266}$	$0.22-0.05\overline{z}^{0.266\,03}$	0.85	1	1	>0
2	$0.245\,15\leqslant\overline{z}<0.372\,6$	247.65	0.193 2	1	0.75	1	<0
3	$0.372\,6\leqslant\overline{z}<0.627\,43$	$269.86+93.18\cdot(\overline{z}-0.372\,6)^{0.859\,4}$	$0.22+0.2\cdot(\overline{z}-0.372\,6)^{0.859\,4}$	1	1	1	=0
4	$0.627\,43\leqslant\overline{z}<0.749\,31$	$282.81-35.16\cdot(\overline{z}-0.627\,4)$	$0.247\,5-0.06\cdot(\overline{z}-0.627\,4)$	1	1	0.75	<0
5	$0.749\,31\leqslant\overline{z}<1$	$281.1\mathrm{e}^{0.975\,9(\overline{z}-0.299\,7)}$	$0.244\,6\mathrm{e}^{(\overline{z}-0.749\,3)}$	1	1	0.85	<0
6	$\overline{z}\geqslant 1$	269.84	0.221 4	0.75	1	1	>0

The elastic fields are calculated for the new transversely isotropic FGM model induced by the point loads f_x and f_z concentrated at the point ($x=y=0, d/h=0.372\,6$). The results along the depth z/h from -0.1 to 1.1 are given in Figs. 2–4, where $E_0 = 1\,\mathrm{GPa}$ for the non-dimensional presentation, $y/h=0$, and $x/h=0.1$, 0.2, 0.3, 0.4, 0.5, 1.0. In the computation, $\delta_{\mathrm{c}} = 0.000\,001$. The constant h is a dimensional factor of the layer thicknesses. The following observations can be made from these figures.

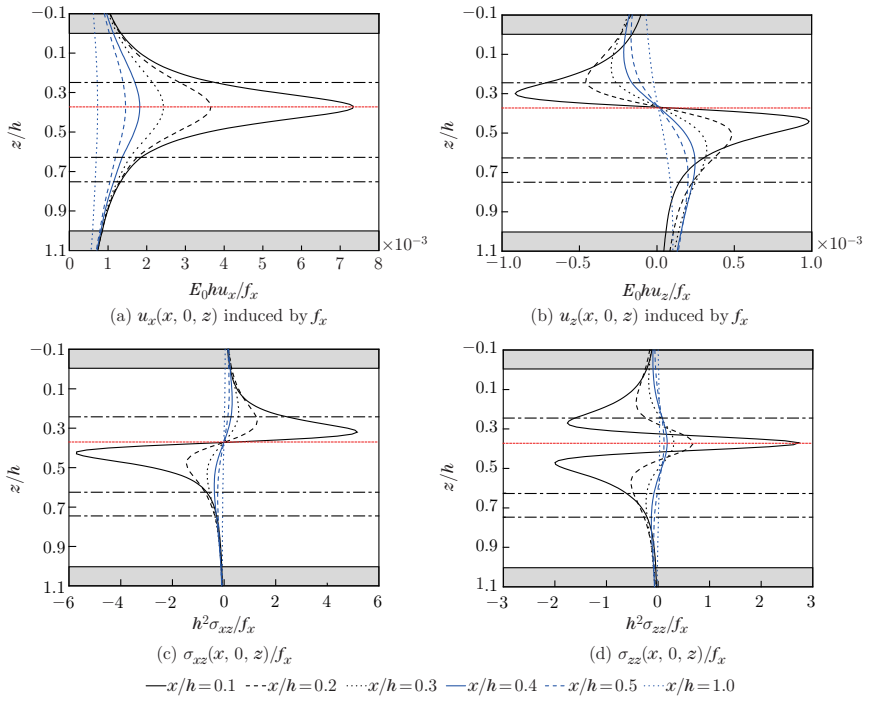

Fig. 2 Variations of displacements and stresses with depth z/h along six locations (x, y) in transversely isotropic FGM model induced by point force f_x, where red dotted line denotes loading plane ($d/h = 0.372\,6$), and each dash-dotted horizontal line stands for interface plane (color online)

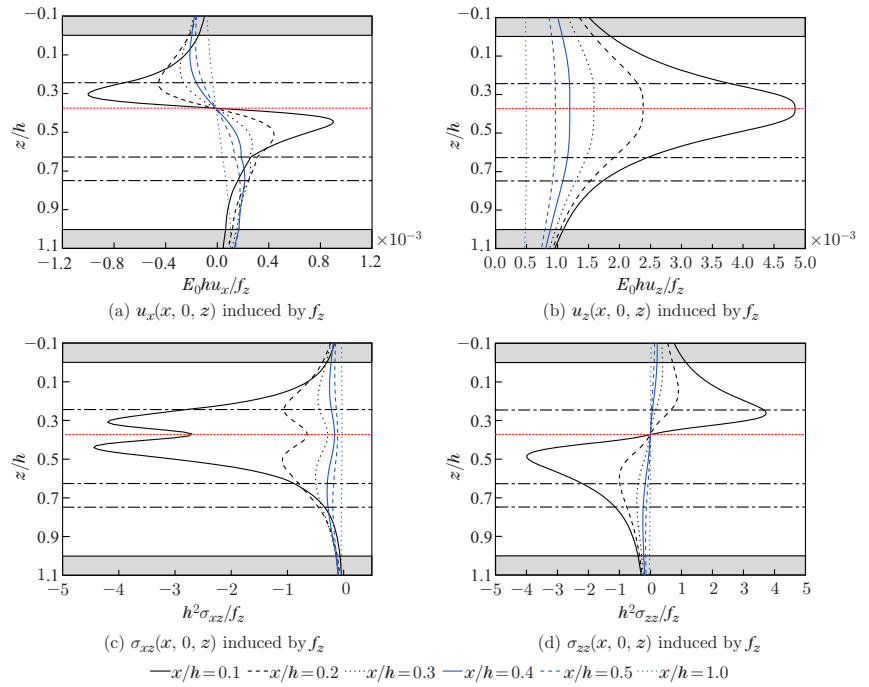

Fig. 3 Variations of displacements and stresses with depth z/h along six locations (x, y) in transversely isotropic FGM model induced by point force f_z, where red dotted line denotes loading plane ($d/h = 0.372\,6$), and each dash-dotted horizontal line stands for interface plane (color online)

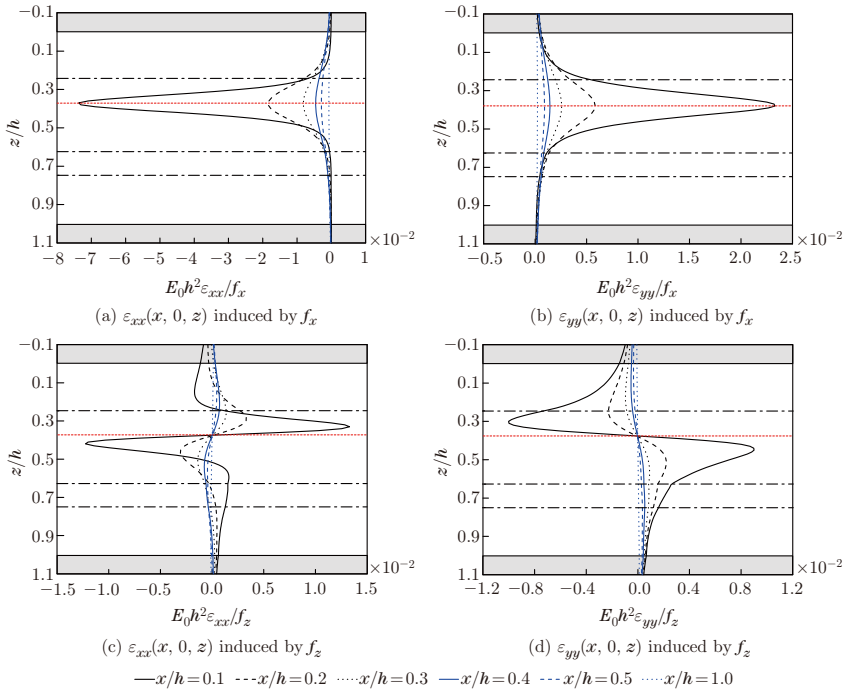

(a) $\varepsilon_{xx}(x, 0, z)$ induced by f_x (b) $\varepsilon_{yy}(x, 0, z)$ induced by f_x

(c) $\varepsilon_{xx}(x, 0, z)$ induced by f_z (d) $\varepsilon_{yy}(x, 0, z)$ induced by f_z

Fig. 4 Variations of two plane normal strains with depth z/h along six locations (x, y) in transversely isotropic FGM model induced by point forces f_x and f_z, where red dotted line denotes loading plane ($d/h = 0.372\,6$), and each dash-dotted horizontal line stands for interface plane (color online)

(i) The displacements u_x and u_z, the vertical stresses σ_{xz} and σ_{zz}, and the plane strains ε_{xx} and ε_{yy} are continuous with the depth z/h.

(ii) The elastic fields at the points approaching the loading point ($x = y = 0, d/h = 0.372\,6$) vary more violently.

(iii) Across the material interfaces between the finite layers or sub-layers, the elastic fields (u_x and u_z, σ_{xz} and σ_{zz}, ε_{xx} and ε_{yy}) are non-smoothly continuous. Because the elastic parameters across the material interfaces do not vary largely, the non-smooth continuity of the elastic fields at the most interfaces is not obvious. However, at some material interfaces, the non-smooth variations can be noticeable. For example, ε_{yy} is non-smoothly continuous across the material interface of the third and fourth layers by f_z along $x/h = 0.1$.

7 Concluding remarks

The paper has presented explicit matrix expressions and precise computation for the point load solutions of 3D elastostatics in an n-layered FGM model with transverse isotropy or isotropy. A general case designed from the isotropic FGM data in Ref. [25] is examined and analyzed. The two kernel 3×3 square matrices $\boldsymbol{\Phi}(\rho, z)$ and $\boldsymbol{\Psi}(\rho, z)$ are dependent on the FGMs and the location of the loading plane, and are independent of the actual loading. If the depth z is located at or closely adjacent to the loading plane and ρ approaches $+\infty$, their asymptotic expressions of all the ten kernel functions are given explicitly as the same as the ten kernel functions associated with the bi-materials of transverse isotropy. Furthermore, the point load solutions of the bi-material are explicitly expressed in closed forms in terms of the elementary

harmonic functions. As a result, the singular terms of the point load solutions for the n-layered FGM model can be isolated and expressed using the closed-form point load solutions of the corresponding bi-materials at the loading plane. The systematic, block, and matrix expressions of the point load solutions enable its precise implementation in the numerical schemes.

The present work can have many extensions and applications as follows: (i) The precise computation method for the point load solutions for an n-layered FGM model can be extended to the cases of an n-layered FGM model subject to other types of loading conditions[26]; (ii) The new point load solutions with closed-form singularity can be implemented as the fundamental singular kernel functions in the boundary element method for more effectively solving complex and practical problems[24].

References

[1] THOMPSON, W. Note on the integration of the equations of equilibrium of an elastic solid. *Cambridge and Dublin Mathematical Journal*, **1**, 97–99 (1848)

[2] BOUSSINESQ, J. *Application des Potentiels à L'étude de L'équilibre et du Mouvement des Solides Élastiques*, Gauther-Villars, Paris (1885)

[3] LOVE, A. E. H. *A Treatise on the Mathematical Theory of Elasticity*, 4th ed., Dover Publications Inc., New York (1882)

[4] MINDLIN, R. D. Force at a point in the interior of a semi-infinite solid. *Physics*, **7**, 195–202 (1936)

[5] RONGVED, L. Force interior to one or two joined semi-infinite solids. *Midwestern Conference on Solid Mechanics*, Purdue University, Lafayette, Indiana, 1–13 (1955)

[6] PLEVAKO, K. P. A point force inside a pair of cohering halfspace. *Osnovaniya Fundamenty i Mekhanika Gruntov*, **3**, 9–11 (1969)

[7] DUNDURS, J. and HETENYI, H. Transmission of force between two semi-infinite solids. *Journal of Applied Mechanics*, **32**, 671–674 (1965)

[8] PAN, Y. C. and CHOU, T. W. Point force solution for an infinite transversely isotropic solid. *Journal of Applied Mechanics*, **43**, 608–612 (1976)

[9] PAN, E. Static Green's functions in multilayered half-spaces. *Applied Mathematical Modelling*, **21**, 509–521 (1997)

[10] PAN, E. Green's functions in layered poroelastic half-spaces. *International Journal for Numerical and Analytical Methods in Geomechanics*, **23**, 1631–1653 (1999)

[11] LIAO, J. J. and WANG, C. D. Elastic solutions for a transversely isotropic half-space subjected to a point load. *International Journal for Numerical and Analytical Methods in Geomechanics*, **22**, 425–447 (1998)

[12] YUE, Z. Q. Elastic fields in two joined transversely isotropic solids due to concentrated forces. *International Journal of Engineering Science*, **33**(3), 351–369 (1995)

[13] BIGONI, D. and CAPUANI, D. Green's function for incremental nonlinear elasticity: shear bands and boundary integral formulation. *Journal of the Mechanics and Physics of Solids*, **50**, 471–500 (2002)

[14] PAN, E. Green's functions for geophysics: a review. *Reports on Progress in Physics*, **82**, 106801 (2019)

[15] MARTIN, P. A., RICHARDSON, J. D., GRAY, L. J., and BERGER, J. R. On Green's function for a three-dimensional exponentially-graded elastic solid. *Proceedings of the Royal Society A-Mathematical, Physical and Engineering Sciences*, **458**, 1931–1947 (2002)

[16] CHAN, Y. S., GRAY, L. J., KAPLAN, T., and PAULINO, G. H. Green's function for a two-dimensional exponentially graded elastic medium. *Proceedings of the Royal Society A-Mathematical, Physical and Engineering Sciences*, **460**, 1689–1706 (2004)

[17] YUE, Z. Q. On generalized Kelvin solutions in a multilayered elastic medium. *Journal of Elasticity*, **40**, 1–43 (1995)

[18] CHEN, X. W. and YUE, Z. Q. A unified mathematical treatment of interfacial edge dislocations in three-dimensional functionally graded materials. *Journal of the Mechanics and Physics of Solids*, **156**, 104471 (2021)

[19] YUE, Z. Q. and WANG, R. Static solutions for transversely isotropic elastic N-layered systems (in Chinese). *Acta Scientiarum Naturalium Universitatis Pekinensis*, **24**(2), 202–211 (1988)

[20] YUE, Z. Q. Yue's solution of classical elasticity in n-layered solids: part 1, mathematical formulation. *Frontiers of Structural and Civil Engineering*, **9**, 215–249 (2015)

[21] YUE, Z. Q. Yue's solution of classical elasticity in n-layered solids: part 2, mathematical verification. *Frontiers of Structural and Civil Engineering*, **9**, 250–285 (2015)

[22] MERKEL, R., KIRCHGESSNER, N., CESA, C. M., and HOFFMANN, B. Cell force microscopy on elastic layers of finite thickness. *Biophysical Journal*, **93**, 3314–3323 (2007)

[23] MALONEY, J. M., WALTON, E. B., BRUCE, C. M., and VAN VLIET, K. J. Influence of finite thickness and stiffness on cellular adhesion-induced deformation of compliant substrata. *Physical Review E*, **78**, 041923 (2008)

[24] XIAO, H. T. and YUE, Z. Q. *Fracture Mechanics in Layered and Graded Materials*: *Analysis Using Boundary Element Methods*, De Gruyter and Higher Education Press, Berlin and Beijing (2014)

[25] SURESH, S. Graded materials for resistance to contact deformation and damage. *Science*, **292**, 2447–2451 (2001)

[26] XIAO, S. and YUE, Z. Q. Matrix Green's function solution of closed-form singularity for functionally graded and transversely isotropic materials under circular ring force vector. *Engineering Analysis with Boundary Elements*, **146**, 569–597 (2023)

Appendix A Constant matrices of elastic parameters

The square matrices $\boldsymbol{C}_{vj}$ and $\boldsymbol{C}_{uj}$ are expressed below,

$$\boldsymbol{C}_{vj}=\begin{pmatrix} 0 & \dfrac{1}{c_{4j}} \\ c_{5j} & 0 \end{pmatrix}, \quad \boldsymbol{C}_{uj}=\begin{pmatrix} 0 & -1 & 0 & \dfrac{1}{c_{4j}} \\ \dfrac{c_{2j}}{c_{3j}} & 0 & \dfrac{1}{c_{3j}} & 0 \\ 0 & 0 & 0 & 1 \\ c_{pj} & 0 & -\dfrac{c_{2j}}{c_{3j}} & 0 \end{pmatrix}. \tag{A1}$$

The square matrices $\boldsymbol{B}_j(\chi)$, $\boldsymbol{C}_j(\chi)$, $\boldsymbol{D}_j(\chi)$, $\boldsymbol{E}_j(\chi)$, $\boldsymbol{C}_{\alpha j}(\chi)$, and $\boldsymbol{C}_{\beta j}(\chi)$ are expressed below,

$$\boldsymbol{B}_j(\chi)=\frac{1}{2}\begin{pmatrix} 1 & \dfrac{1}{c_{4j}\chi} \\ c_{4j}\chi & 1 \end{pmatrix}, \tag{A2}$$

$$\boldsymbol{C}_j(\chi)=\frac{1}{2(r_{1j}^2-r_{2j}^2)\chi}\begin{pmatrix} \chi^3+\dfrac{c_{2j}}{c_{3j}}\chi & -\Big(\chi^2+\dfrac{c_{2j}}{c_{3j}}\Big) & -\dfrac{c_{2j}+c_{4j}}{c_{3j}c_{4j}}\chi & \dfrac{1}{c_{4j}}\chi^2-\dfrac{1}{c_{3j}} \\ \dfrac{c_{2j}}{c_{3j}}\chi^2+\dfrac{c_{1j}}{c_{3j}} & \chi^3+c_{qj}\chi & \dfrac{1}{c_{3j}}\chi^2-\dfrac{c_{1j}}{c_{3j}c_{4j}} & \dfrac{c_{2j}+c_{4j}}{c_{3j}c_{4j}}\chi \\ c_{pj}\chi & -c_{pj} & \chi^3+c_{qj}\chi & \chi^2+\dfrac{c_{2j}}{c_{3j}} \\ c_{pj}\chi^2 & -c_{pj}\chi & -\Big(\dfrac{c_{2j}}{c_{3j}}\chi^2+\dfrac{c_{1j}}{c_{3j}}\Big) & \chi^3+\dfrac{c_{2j}}{c_{3j}}\chi \end{pmatrix}, \tag{A3}$$

$$\boldsymbol{D}_j(\chi)=\frac{1}{2}\begin{pmatrix} 1 & -\dfrac{c_{4j}}{c_{3j}\chi^3} & 0 & \dfrac{c_{2j}+3c_{4j}}{2c_{3j}c_{4j}\chi^3} \\ -\dfrac{c_{4j}}{c_{3j}\chi} & 1 & \dfrac{c_{2j}+3c_{4j}}{2c_{3j}c_{4j}\chi} & 0 \\ 0 & \dfrac{2c_{4j}(c_{2j}+c_{4j})}{c_{4j}\chi^3} & 1 & \dfrac{c_{4j}}{c_{3j}\chi^3} \\ \dfrac{2c_{4j}(c_{2j}+c_{4j})}{c_{4j}\chi} & 0 & \dfrac{c_{4j}}{c_{3j}\chi} & 1 \end{pmatrix}, \tag{A4}$$

$$\boldsymbol{E}_j(\chi)=\frac{c_{2j}+c_{4j}}{2c_{3j}\chi^2}\begin{pmatrix} 1 & -\dfrac{1}{\chi} & -\dfrac{1}{2c_{4j}} & \dfrac{1}{2c_{4j}\chi} \\ \chi & -1 & -\dfrac{\chi}{2c_{4j}} & \dfrac{1}{2c_{4j}} \\ 2c_{4j} & -\dfrac{2c_{4j}}{\chi} & -1 & \dfrac{1}{\chi} \\ 2c_{4j}\chi & -2c_{4j} & -\chi & 1 \end{pmatrix}, \tag{A5}$$

$$\boldsymbol{C}_{\alpha j}(\chi)=\frac{1}{4c_{aj}}\begin{pmatrix} 2c_{aj} & \Big(-1+\dfrac{c_{2j}}{c_{sj}}\Big)\chi & 0 & \Big(\dfrac{1}{c_{4j}}+\dfrac{1}{c_{sj}}\Big)\chi \\ \Big(\dfrac{c_{2j}}{c_{3j}}-\dfrac{c_{1j}}{c_{sj}}\Big)\chi & 2c_{aj} & \Big(\dfrac{1}{c_{3j}}+\dfrac{c_{1j}}{c_{sj}c_{4j}}\Big)\chi & 0 \\ 0 & \dfrac{c_{pj}}{c_{aj}^2+c_{bj}^2}\chi & 2c_{aj} & \Big(1-\dfrac{c_{2j}}{c_{sj}}\Big)\chi \\ c_{pj}\chi & 0 & -\Big(\dfrac{c_{2j}}{c_{3j}}-\dfrac{c_{1j}}{c_{sj}}\Big)\chi & 2c_{aj} \end{pmatrix}, \tag{A6}$$

$$\boldsymbol{C}_{\beta j}(\chi)=\frac{1}{4c_{aj}c_{bj}}$$

$$\cdot\begin{pmatrix} \dfrac{c_{2j}}{c_{3j}}+c_{aj}^2-c_{bj}^2 & -\Big(c_{aj}+\dfrac{c_{2j}c_{aj}}{c_{sj}}\Big)\chi & -\dfrac{c_{2j}+c_{4j}}{c_{3j}c_{4j}} & \Big(\dfrac{c_{aj}}{c_{4j}}-\dfrac{c_{aj}}{c_{sj}}\Big)\chi \\ \Big(\dfrac{c_{aj}c_{2j}}{c_{3j}}+\dfrac{c_{aj}c_{1j}}{c_{sj}}\Big)\chi & c_{aj}^2-c_{bj}^2+c_{qj} & \Big(\dfrac{c_{aj}}{c_{3j}}-\dfrac{c_{aj}c_{1j}}{c_{sj}c_{4j}}\Big)\chi & \dfrac{c_{2j}+c_{4j}}{c_{3j}c_{4j}} \\ c_{pj} & -\dfrac{c_{aj}c_{pj}}{c_{aj}^2+c_{bj}^2}\chi & c_{aj}^2-c_{bj}^2+c_{qj} & \Big(c_{aj}+\dfrac{c_{2j}c_{aj}}{c_{sj}}\Big)\chi \\ c_{aj}c_{pj}\chi & -c_{pj} & -\Big(\dfrac{c_{aj}c_{2j}}{c_{3j}}+\dfrac{c_{aj}c_{1j}}{c_{sj}}\Big)\chi & \dfrac{c_{2j}}{c_{3j}}+c_{aj}^2-c_{bj}^2 \end{pmatrix}, \tag{A7}$$

where c_{aj} and c_{bj} are presented in Appendix B.

In the above expressions, c_{pj}, c_{qj}, and c_{sj} are expressed as

$$c_{pj}=c_{1j}-\frac{c_{2j}^2}{c_{3j}},\quad c_{qj}=\frac{c_{2j}^2+c_{2j}c_{4j}-c_{1j}c_{3j}}{c_{3j}c_{4j}},\quad c_{sj}=c_{3j}(c_{aj}^2+c_{bj}^2). \tag{A8}$$

The matrices $\boldsymbol{q}_0$, $\boldsymbol{p}_{n+1}$, $\boldsymbol{P}_{q0}$, and $\boldsymbol{P}_{p(n+1)}$ are expressed below,

$$\boldsymbol{q}_0=\begin{pmatrix}1 & -\dfrac{1}{c_{40}\gamma_{00}}\end{pmatrix},\quad \boldsymbol{p}_{n+1}=\begin{pmatrix}1 & \dfrac{1}{c_{4(n+1)}\gamma_{0(n+1)}}\end{pmatrix},$$

$$\boldsymbol{P}_{q0}=\begin{pmatrix} 2c_{a0} & 1-\dfrac{c_{20}}{\sqrt{c_{10}c_{30}}} & 0 & -\dfrac{1}{c_{40}}-\dfrac{1}{\sqrt{c_{10}c_{30}}} \\ \sqrt{\dfrac{c_{10}}{c_{30}}}-\dfrac{c_{20}}{c_{30}} & 2c_{a0} & -\dfrac{1}{c_{30}}-\dfrac{\sqrt{c_{10}c_{30}}}{c_{30}c_{40}} & 0 \end{pmatrix},$$

$$\boldsymbol{P}_{p(n+1)} = \begin{pmatrix} 2c_{a(n+1)} & \dfrac{c_{2(n+1)}}{\sqrt{c_{1(n+1)}c_{3(n+1)}}}-1 & 0 & \dfrac{1}{c_{4(n+1)}}+\dfrac{1}{\sqrt{c_{1(n+1)}c_{3(n+1)}}} \\ \dfrac{c_{2(n+1)}}{c_{3(n+1)}}-\sqrt{\dfrac{c_{1(n+1)}}{c_{3(n+1)}}} & 2c_{a(n+1)} & \dfrac{1}{c_{3(n+1)}}+\dfrac{\sqrt{c_{1(n+1)}c_{3(n+1)}}}{c_{3(n+1)}c_{4(n+1)}} & 0 \end{pmatrix}. \tag{A9}$$

Appendix B Characteristic roots of transversely isotropic materials

The material characteristic roots γ_{0j}, γ_{1j}, γ_{2j}, and γ_{3j} are defined as follows:

$$\begin{cases} \gamma_{0j} = \sqrt{c_{5j}/c_{4j}}, \\ \gamma_{1j} = c_{aj} + c_{bj} > 0, \quad \gamma_{2j} = c_{aj} - c_{bj} > 0 \quad \text{for} \quad \Delta_j > 0, \\ \gamma_{1j} = c_{aj} + \mathrm{i}c_{bj}, \quad \gamma_{2j} = c_{aj} - \mathrm{i}c_{bj} \quad \text{for} \quad \Delta_j < 0, \\ \gamma_{3j} = (c_{1j}/c_{3j})^{\frac{1}{4}} \quad \text{for} \quad \Delta_j = 0, \end{cases} \tag{B1}$$

where

$$\begin{cases} c_{aj} = \dfrac{\sqrt{(\sqrt{c_{1j}c_{3j}}+c_{2j}+2c_{4j})(\sqrt{c_{1j}c_{3j}}-c_{2j})}}{2\sqrt{c_{3j}c_{4j}}}, \\ c_{bj} = \dfrac{\sqrt{(\sqrt{c_{1j}c_{3j}}+c_{2j})|\Delta_j|}}{2\sqrt{c_{3j}c_{4j}}}, \quad \Delta_j = \sqrt{c_{1j}c_{3j}} - c_{2j} - 2c_{4j}. \end{cases} \tag{B2}$$

Appendix C Specific solution of $\boldsymbol{V}(z)$ in terms of $\boldsymbol{G}_v$ for $-\infty < z \leqslant d^-$

Using Eq. (12), the general solution of $\boldsymbol{V}(z)$ for the 0th and $(n+1)$th layers can be expressed in terms of $\boldsymbol{V}(H_0^-)$ and $\boldsymbol{V}(H_n^+)$ as follows:

$$\begin{cases} \boldsymbol{V}(z) = \mathrm{e}^{-\gamma_{00}\rho(H_0-z)}\boldsymbol{B}_0(\gamma_{00})\boldsymbol{V}(H_0^-), \quad \boldsymbol{q}_0\boldsymbol{V}(H_0^-) = 0, \\ \boldsymbol{V}(z) = \mathrm{e}^{-\gamma_{0(n+1)}\rho(z-H_n)}\boldsymbol{B}_{n+1}(-\gamma_{0(n+1)})\boldsymbol{V}(H_n^-), \quad \boldsymbol{p}_{n+1}\boldsymbol{V}(H_n^+) = 0, \end{cases} \tag{C1}$$

where $\boldsymbol{q}_0$, $\boldsymbol{p}_{n+1}$, $\boldsymbol{B}_0(\chi)$, and $\boldsymbol{B}_{n+1}(\chi)$ are given in Appendix A.

Similarly, the general solution of $\boldsymbol{V}(z)$ for the jth layer can be expressed in terms of $\boldsymbol{V}(H_{j-1}^+)$ as follows:

$$\boldsymbol{V}(z) = \begin{cases} \mathrm{e}^{\gamma_{0j}\rho(z-H_{j-1})}\boldsymbol{A}_j^p(z-H_{j-1})\boldsymbol{V}(H_{j-1}^+) \quad \text{for} \quad H_{j-1}^+ \leqslant z \leqslant H_j^-, \quad 1 \leqslant j \leqslant k-1, \\ \mathrm{e}^{\gamma_{0k}\rho(z-H_{k-1})}\boldsymbol{A}_k^p(z-H_{k-1})\boldsymbol{V}(H_{k-1}^+) \quad \text{for} \quad H_{k-1}^+ \leqslant z \leqslant d^-, \quad j = k, \\ \mathrm{e}^{\gamma_{0k}\rho(z-H_{k-1})}\boldsymbol{A}_k^p(z-H_{k-1})\boldsymbol{V}(H_{k-1}^+) \\ \quad - \mathrm{e}^{\gamma_{0k}\rho(z-d)}\boldsymbol{A}_k^p(z-d)\boldsymbol{G}_v \quad \text{for} \quad d^+ \leqslant z \leqslant H_k^-, \quad j = k, \\ \mathrm{e}^{\gamma_{0j}\rho(z-H_{j-1})}\boldsymbol{A}_j^p(z-H_{j-1})\boldsymbol{V}(H_{j-1}^+) \quad \text{for} \quad H_{j-1}^+ \leqslant z \leqslant H_j^-, \quad k+1 \leqslant j \leqslant n, \end{cases} \tag{C2}$$

where $\boldsymbol{A}_j^p(s)$ contains only the function of exponential decrease and is given in Eq. (21).

Using the interface condition (17), the general solution of $\boldsymbol{V}(z)$ can be expressed in terms of $\boldsymbol{V}(H_0)$ and $\boldsymbol{G}_v$ as follows.

(i) For $H_0 \leqslant z \leqslant d$ and $0 < j \leqslant k$, we have

$$\boldsymbol{V}(z) = \mathrm{e}^{\gamma_{0j}\rho(z-H_{j-1})+\gamma_{0(j-1)}\rho h_{j-1}+\cdots+\gamma_{01}\rho h_1}\boldsymbol{A}_j^p(z-H_{j-1})\boldsymbol{A}_{j-1}^p(h_{j-1})\cdots\boldsymbol{A}_1^p(h_1)\boldsymbol{V}(H_0). \tag{C3a}$$

(ii) For $d \leqslant z \leqslant H_n$ and $k \leqslant j \leqslant n$, we have

$$\begin{aligned} \boldsymbol{V}(z) = {} & \mathrm{e}^{\gamma_{0j}\rho(z-H_{j-1})+\gamma_{0(j-1)}\rho h_{j-1}+\cdots+\gamma_{01}\rho h_1}\boldsymbol{A}_j^p(z-H_{j-1})\boldsymbol{A}_{j-1}^p(h_{j-1})\cdots\boldsymbol{A}_1^p(h_1)\boldsymbol{V}(H_0) \\ & - \mathrm{e}^{\gamma_{0j}\rho(z-H_{j-1})+\gamma_{0(j-1)}\rho h_{j-1}+\cdots+\gamma_{0k}\rho(H_k-d)} \\ & \cdot \boldsymbol{A}_j^p(z-H_{j-1})\boldsymbol{A}_{j-1}^p(h_{j-1})\cdots\boldsymbol{A}_{k+1}^p(h_{k+1})\boldsymbol{A}_k^p(H_k-d)\boldsymbol{G}_v. \end{aligned} \tag{C3b}$$

In addition, the linear equation between $\boldsymbol{V}(H_n)$ and $\boldsymbol{V}(H_0)$ can be obtained as follows:

$$\begin{aligned}\boldsymbol{V}(H_n) = {} & \mathrm{e}^{\gamma_{0n}\rho h_n+\gamma_{0(n-1)}\rho h_{n-1}+\cdots+\gamma_{01}\rho h_1}\boldsymbol{A}_n^p(h_n)\boldsymbol{A}_{n-1}^p(h_{n-1})\cdots\boldsymbol{A}_1^p(h_1)\boldsymbol{V}(H_0)\\ & - \mathrm{e}^{\gamma_{0n}\rho h_n+\gamma_{0(n-1)}\rho h_{n-1}+\cdots+\gamma_{0(k+1)}\rho h_{k+1}+\gamma_{0k}\rho(H_k-d)}\\ & \cdot \boldsymbol{A}_n^p(h_n)\boldsymbol{A}_{n-1}^p(h_{n-1})\cdots\boldsymbol{A}_{k+1}^p(h_{k+1})\boldsymbol{A}_k^p(H_k-d)\boldsymbol{G}_v. \end{aligned} \tag{C4}$$

Using Eqs. (C1) and (C4), we can have the following boundary equations governing $\boldsymbol{V}(H_0)$:

$$\begin{aligned}& \begin{pmatrix} \boldsymbol{q}_0 \\ \boldsymbol{p}_{n+1}\boldsymbol{A}_n^p(h_n)\boldsymbol{A}_{n-1}^p(h_{n-1})\cdots\boldsymbol{A}_1^p(h_1)\end{pmatrix}\boldsymbol{V}(H_0)\\ = {} & \mathrm{e}^{-\gamma_{0k}\rho(d-H_{k-1})-\gamma_{0(k-1)}\rho h_{k-1}-\cdots-\gamma_{01}\rho h_1}\\ & \cdot \begin{pmatrix} \boldsymbol{0} \\ \boldsymbol{p}_{n+1}\boldsymbol{A}_n^p(h_n)\boldsymbol{A}_{n-1}^p(h_{n-1})\cdots\boldsymbol{A}_{k+1}^p(h_{k+1})\boldsymbol{A}_k^p(H_{k-1}-d)\end{pmatrix}\boldsymbol{G}_v. \end{aligned} \tag{C5}$$

The specific solution of $\boldsymbol{V}(H_0)$ can be expressed as

$$\boldsymbol{V}(H_0) = \mathrm{e}^{-\gamma_{01}\rho h_1-\gamma_{02}\rho h_2-\cdots-\gamma_{0(k-1)}\rho h_{k-1}-\gamma_{0k}\rho(d-H_{k-1})}\boldsymbol{N}_{Ap}\boldsymbol{G}_v, \tag{C6}$$

where $\boldsymbol{N}_{Ap}$ is given in Eq. (25).

Substitute Eq. (C6) into Eqs. (C1) and (C3a) and (C3b). Then, the specific solution of $\boldsymbol{V}(z)$ in terms of $\boldsymbol{G}_v$ (see Eqs. (19) and (20)) for $-\infty < z \leqslant d^-$ can be obtained.